

# Modeling and Optimal Low-Power On–Off Control of Thin-Film Piezoelectric Rotational Actuators

Biju Edamana, Bongsu Hahn, Jeffrey S. Pulskamp, Ronald G. Polcawich, and Kenn Oldham, *Member, IEEE*

**Abstract**—A novel open-loop minimal energy on–off servo system and control strategy are described for ensuring specified displacements from new microscale piezoelectric rotational joints under extremely strict power budgets. The rotational joints are driven by thin-film lead–zirconate–titanate actuators and are targeted for use in autonomous terrestrial microrobots. A lumped-parameter, second-order model of anticipated joint behavior is utilized to estimate the natural frequency and damping ratio of the robot joints, which, in turn, are used to identify necessary sampling rates and switching drive circuit parameters for implementation of on–off control. An identified model of leg joint behavior is then used to both verify lumped-parameter modeling and to optimize on–off input sequences to the rotary joint. The optimization procedure incorporates energy costs from both switching and holding an input voltage on microactuators that behave as a capacitive load, while ensuring that specified final states of a dynamic system are achieved at a specified point in time. Optimization is done via a new application of binary programming. In addition, modest robustness of the system response to parameter variation can be produced during control sequence generation. Optimized input sequences are applied to both macroscale piezoelectric actuators and to prototype thin-film piezoelectric leg joints, and show that specified actuator motions can be achieved with energy consumption of less than  $5 \mu\text{J}$  per movement.

**Index Terms**—Integer programming, microactuators, microelectromechanical devices, on–off control, piezoelectric devices, switched systems.

## I. INTRODUCTION

THE OPPORTUNITY to dramatically reduce the size of actuators and sensors through microelectromechanical system (MEMS) technology makes possible a variety of miniature autonomous devices, such as unattended sensor nodes or mobile microrobots. However, in autonomous operation, taking full advantage of the small size of MEMS mechanisms requires that one also ensure small size of power sources, circuitry, and other subsystems required to operate the central MEMS component.

Manuscript received December 11, 2009; revised April 7, 2010; accepted May 8, 2010. Date of publication July 23, 2010; date of current version August 30, 2011. Recommended by Technical Editor G. Alici. This work was supported in part by the U.S. Defense Advanced Research Projects Agency under Grant HR0011-08-1-0040 and in part by the U.S. Army Research Office under Grant W911QX-07-C-0072.

B. Edamana, B. Hahn, and K. Oldham are with the Department of Mechanical Engineering, University of Michigan, Ann Arbor, MI 48109 USA (e-mail: bij@umich.edu; suhahn@umich.edu; oldham@umich.edu).

J. S. Pulskamp and R. G. Polcawich are with the Sensors and Electron Devices Directorate, U.S. Army Research Laboratory, Adelphi, MD 20783 USA (e-mail: jeffrey.pulskamp@arl.army.mil; ronald.polcawich@arl.army.mil).

Color versions of one or more of the figures in this paper are available online at <http://ieeexplore.ieee.org>.

Digital Object Identifier 10.1109/TMECH.2010.2053041

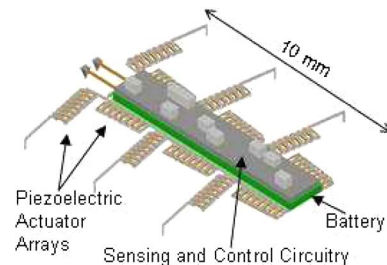


Fig. 1. Concept drawing of an autonomous microrobot based on thin-film piezoelectric actuator joint arrays.

One opportunity for reducing power needs of MEMS microactuators is aggressive reduction in power needed to perform controlled actuator movements. A new optimal on–off switching controller, as described in this paper, is a promising method for meeting especially strict constraints on power consumption. This method accommodates both efficient actuator drive circuitry and minimizes servo system energy usage to accomplish prescribed movements.

Especially severe power constraints are faced when MEMS actuators are intended to actuate autonomous microrobots, on the scale of one centimeter or smaller, as in the concept drawing shown in Fig. 1. While a few microrobots at this scale have been demonstrated in autonomous or tethered operation, their mobility has been limited by the need to either carry a large-power supply, by limited actuation force at low power, or by the need to operate on a dedicated substrate. Several previous robots have been based on thermal actuation, but the large-power consumption of thermal actuators permits only single degree of freedom, short-displacement leg joints in order to carry large-battery mass [1]–[3]. In contrast, microrobots based on electrostatic actuation can be powered with much smaller power supplies, but electrostatic actuators require very large areas to produce significant force, permitting only a few limbs or degrees of freedom per robot; alternatively, electrostatic microrobots may depend on a specialized substrate to deliver power, limiting autonomy to small areas [4]–[6].

Thin-film piezoelectric actuators, in contrast, are capable of delivering much larger forces than electrostatic actuators with much smaller power requirements than thermal actuators, or other potential robotic actuators, such as electromagnetic actuators or shape-memory alloys. A thin-film lateral actuator has been previously demonstrated capable of generating up to  $3 \times 10^{-9}$  N·m of work in a  $500 \mu\text{m} \times 100 \mu\text{m}$  area, and this paper may be leveraged using silicon microstructures to generate rotational motion of  $3^\circ$  or more from a single such actuator at 20 V [7]. Operated in multiactuator arrays, these actuators can

generate large-angle rotations of microrobotic leg joints. A typical array, as discussed in this paper, would have a capacitance of less than 1 nF, corresponding to intrinsic energy consumption of less than 1  $\mu$ J each time an actuator is charged to an operating voltage on the order of 20 to 30 V. Furthermore, integrated with silicon structures, they could potentially carry between 5 and 50 mg payloads per leg [8], [9]. However, even with state-of-the-art thin-film battery or solar power sources [10], [11], the power budget per leg at that payload capacity is on the order of a few hundred microwatts to a few milliwatts, making extremely low-power servo systems a necessity for microrobots based on these actuators. In addition, reduction in power requirements to control piezoelectric actuators could be useful to slightly larger miniature robots [12], [13], where energy constraints are not as severe, but servo power reduction still allows for larger payloads.

Unfortunately, controlling the motion of a robotic appendage, as to move a leg to a specified angle in a given step, introduces significant additional power consumption beyond that of the actuator itself. Existing operational amplifiers operating in the range of 20 to 30 V consume at least 400  $\mu$ W in quiescent power, and in a typical analog amplifier circuit for piezoelectric actuators, as much as 95% of the power used by the actuator may be wasted [14]. As a result, switching interface circuits between a high-voltage supply and the piezoelectric actuator are desirable, with motion control typically applied using pulsewidth modulation (PWM). However, PWM requires very high switching frequencies, which dramatically increases power consumption when driving a capacitive load. Charge recovery, such as that developed by Campolo *et al.* [15], is one method for reducing this energy, use is through, but inductor sizes necessary for effective charge recovery can be excessively large and energy losses are still most prevalent during switching, although these losses are reduced. Another way of rotating through fixed angles is to make use of mechanical stops [16], [17]; the drawback in this method is that there is only one possible angle of rotation. Meanwhile, power consumption of sensor circuitry required for feedback also greatly exceeds power consumption of thin-film piezoelectric actuators, such that open-loop control may be necessary to meet especially strict power limits.

Open-loop on-off control, using a limited number of switching transitions per actuator movement, can produce regulated movements with extremely small energy usage, provided that on-off switching times are chosen carefully and a reasonable model of the system is available. Previous optimization techniques for on-off control schemes have minimized the time to reach a desired set of system states [18], or the amount of time spent with an “on” input to reach a desired set of states at a specified time [19], [20], but these approaches do not account for switching costs, such as energy usage to charge a capacitive actuator. Alternatively, full-fledged hybrid system models can be used to approach on-off control design [21], [22], but this may be an unnecessarily complex approach when only two input selections are available.

This paper presents a model for a piezoelectric microrobotic leg joint, a low-power switching circuit for control of the joint, and an optimization procedure for generating minimum energy on-off input sequences to direct the resulting motion. The open-

loop optimal on-off switching sequences drive a set of initial states to a desired set of output states, while minimizing total energy usage. The optimization procedure is based on binary programming, which permits a simpler optimization procedure than that of full-fledged hybrid systems approaches, but allows switching costs to be incorporated into the optimization cost, unlike previous controllers designed specifically for on-off sequence optimization. Applied to the piezoelectric microactuator arrays in a novel rotational joint configuration, the controller can drive comparatively large displacements to specified angles with just a few on-off switching transitions and extremely low-power consumption. The control inputs are applied to the piezoelectric actuators through a low-power switching drive circuit, to further reduce system power consumption.

Following this introduction, Section II introduces the thin-film piezoelectric actuator and leg joint models. Section III describes the design of a low-power switching circuit for interfacing. Section IV describes the on-off input sequence optimization procedure and a simulational study. Section VI provides experimental results from the on-off controller using a low-power switching drive circuit. Section VII discusses implications for future low-power microrobot operation and concludes the paper.

## II. ACTUATOR DESIGN AND MODELING

### A. Individual Flexure and Actuators

The large-angle, rotational joint to be controlled consists of a series of eight elastic silicon flexures between rigid silicon links developed at the U.S. Army Research Laboratory, as shown in Fig. 2. Each link contains a thin-film piezoelectric actuator that applies a bending moment to one of the silicon flexures via a thin silicon tether. Net rotation at the tip of the joint is the sum of the rotation angles of each flexure-actuator pair.

Each flexure in the array is a thin silicon beam that experiences elastic deflection due to the moment generated by the actuator force offset from the tip of the actuator by distance  $L_{act}$ , as shown in Fig. 2(c2) and (c3). The rotational stiffness of each link is given by the equation

$$k_{\theta} = \frac{Etw_f^3}{12L_f} \quad (1)$$

where  $E$  is the elastic modulus of silicon,  $t$  is the thickness of the silicon flexures,  $w_f$  is the flexure width, and  $L_f$  is the flexure length. Flexure parameters as described and fabricated are shown in Table I. While the nominal flexure thickness was to be 10  $\mu$ m in the legs tested, excessive undercut of the silicon structures during deep reactive ion etching resulted in thin silicon structures (flexures and tethers) having a thickness of only approximately 6  $\mu$ m, leading to a somewhat less stiff joint structure than anticipated.

The piezoelectric actuators consist of bend-up and bend-down unimorph segments connected in series to produce net in-plane displacement at the actuator tip, as shown in Fig. 3. The bend-up unimorph segments consist of a silicon dioxide base layer that sets the height of the neutral bending axis below the piezoelectric film, a bottom platinum electrode, a lead-zirconate-titanate (PZT) piezoelectric thin film, and a top platinum electrode. The

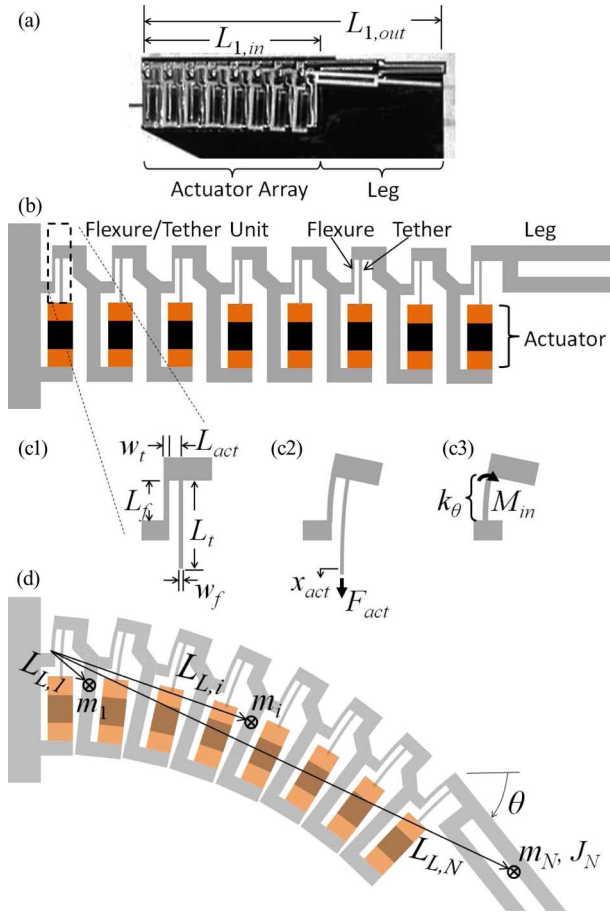


Fig. 2. Multiactuator leg joint. (a) Optical photograph. (b) Schematic drawing of components. (c) Link dimensions. (c2) Force and displacement at actuator tip. (c3) Equivalent bending moment model. (d) Mass and inertia definitions in deflected state.

TABLE I  
FLEXURE AND ACTUATOR PARAMETERS

Parameter	Label	Units	Nominal Value	Fabricated Value
Elastic Modulus (Si)	$E$	GPa	170	170
Device Thickness	$t$	$\mu\text{m}$	10	6
Flexure Width	$w_f$	$\mu\text{m}$	7	6.7
Flexure Length	$L_f$	$\mu\text{m}$	120	120
Spring Constant	$k_\theta$	$\mu\text{N/rad/s}$	0.38	0.23
Actuator Offset	$L_{act}$	$\mu\text{m}$	12	12
Tether Width	$w_t$	$\mu\text{m}$	5	4.7
Tether Length	$L_t$	$\mu\text{m}$	292	292

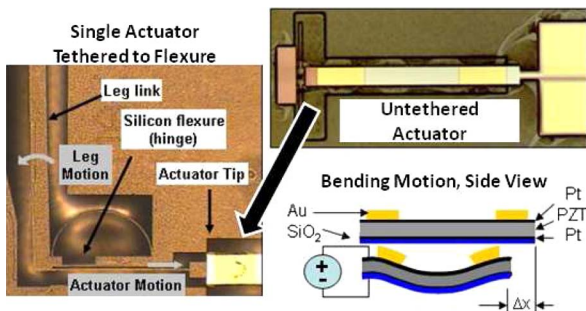


Fig. 3. Schematic diagram and optical images of an individual thin-film piezoelectric lateral actuator, alone and tethered to single flexure.

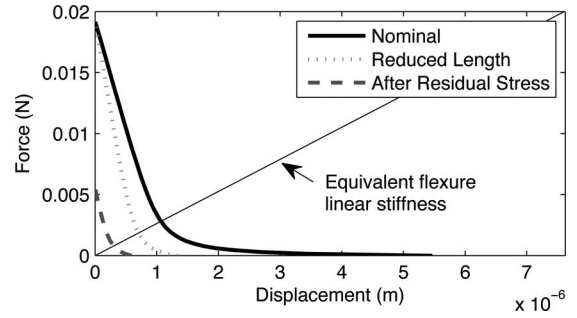


Fig. 4. Force versus displacement curve of thin-film piezoelectric actuators at 20 V, nominal model from [7] and with effects of fabrication limitations.

bend-down unimorph segments have an additional gold film added, to raise the neutral bending axis of the structure above the midline of the PZT film in that segment. The net effect is to produce in-plane lateral actuators with the large-force capacity of piezoelectric actuation and increased stroke length due to nonlinearity of the bend-up and bend-down structure. A full force–displacement model of these actuators was previously described in [7], and the resulting force–displacement curve for a nominal 500- $\mu\text{m}$ -long, 100- $\mu\text{m}$ -wide actuator at 20 V is shown in Fig. 4. The effective electroactive piezoelectric strain coefficient ( $d_{31,\text{eff}}$ ) for these actuators at 20 V was approximately  $-60 \text{ pm/V}$ , while the dielectric coefficient was approximately 230.

Unfortunately, while the nominal force–displacement of the actuators, as designed and tested in the previous work, would generate greater than  $3^\circ$  of rotation at each link, flaws during the microfabrication process greatly reduced the force–displacement capabilities of the actuators tested here. Namely, insufficient undercut of the silicon layer beneath the actuators reduced their length to only about 440  $\mu\text{m}$ , and residual stress in the thin film layers, particularly the gold films used to generate bend-down motion at the outer segments of the actuator, has the effect of shifting the force–displacement curve away from its nominal position. When the observed length of the actuators following fabrication and estimated residual stress levels are incorporated in the actuator models, the expected force–displacement curve diminishes, as shown in the additional curves in Fig. 4. While this decrease in performance is not a significant factor in verifying controller performance and power consumption, reducing negative effects of residual stress and better regulating actuator length and stiffness will be necessary to achieve truly large range-of-motion microrobotic joints.

Conversion of the actuator force as a function of displacement to the moment on the flexures as a function of flexure rotation depends, first, on the offset between the actuator tether and the elastic flexure in each link, and second, on the stiffness of the tether itself. For a given offset  $L_{act}$ , the resulting moment due to the actuation force  $F_{act}$  is given by

$$M_{in} = F_{act} L_{act}. \quad (2)$$

The static lateral displacement at the tip of each actuator  $x_{act}$  is dependent on the force  $F_{act}$  that the actuator is applying, and is given by the force–displacement curve for the thin-film

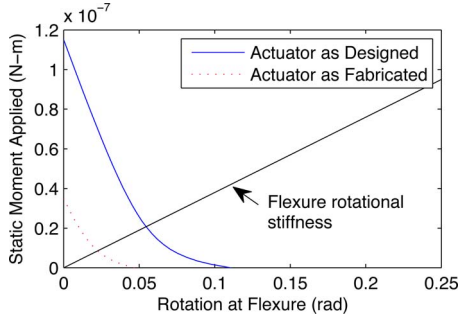


Fig. 5. Static applied actuator moment at 20 V versus rotation angle at silicon flexures, based on nominal actuator design and taking into account all fabrication limitations.

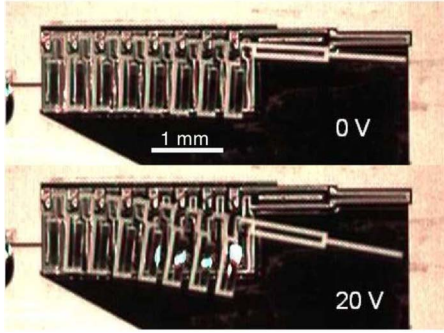


Fig. 6. Sample image of leg joint at 0 and 20 V.

piezoelectric actuators. The actuator tip displacement is also equal to displacement due to rotation of the leg link ( $L_{act}$  times rotation angle for the link to which it attached) plus any axial stretching in the tether  $x_t$ . A corresponding static rotation  $\theta_{max}(M)$  for each leg link can then be estimated from

$$\theta_{max}(M_{in}) = \frac{x_{act}(F_{act}) - x_t}{L_{act}} \quad (3)$$

where  $x_t$  is given by

$$x_t = \frac{F_{act}L_t}{Ew_t t} \quad (4)$$

with  $L_t$  being the length of the tether and  $w_t$  is the tether width.

This rotation must match that of the flexures, such that the actual static rotation of each link occurs at the point, where the actuation moment as a function of rotation intersects the rotary stiffness curve of the flexures, as shown in Fig. 5. Had the actuators been functioning at full-nominal performance as discussed with respect to the force–displacement curve in Fig. 4, anticipated rotation angle of each link for a 20 V input was to be approximately  $3^\circ$  or 0.052 rad. At the reduced actuation capacity of the actuators as formed, we find rotation angles of approximately  $1^\circ$  or 0.021 rad per link, and  $8^\circ$  per leg joint. Experimentally, a rotation of  $7.5^\circ$  from the entire joint is observed at 20 V, with a sample rotary leg joint at 0 and 20 V shown in Fig. 6. Again, this reduction in displacement is primarily a result of underetching of silicon along the actuator length, and residual stress prestressing the actuator against the direction of desired motion.

## B. Lumped-Parameter Dynamics

Although on–off input sequence optimization is ultimately performed using an identified model of system dynamics, an analytical model for joint dynamics is useful for both designing leg joint design and specifying reasonable sampling times and switching circuit parameters when implementing the on–off controller. While the large deflection leg joints consist of several flexures and rigid links in series, the small mass of the intermediate links allows actuator dynamics to be described with reasonable accuracy using a lumped-parameter second-order model, particularly for small displacement of approximately  $10^\circ$  or less, where small angle sine and cosine approximations are effective. The resulting second-order model has the form as follows:

$$J_{tot}\ddot{\theta}_{tot} + b_{tot}\dot{\theta}_{tot} + k_{tot}\theta = Gu(t) \quad (5)$$

where  $J_{tot}$  is the total rotary inertia of the system,  $b_{tot}$  is a rotational damping coefficient,  $k_{tot}$  is the equivalent total spring stiffness,  $G$  is the equivalent actuation moment per volt, and  $u(t)$  is the applied input voltage.

The input to the system is treated as constant when voltage is applied, taken as the moment applied by the actuator when the moment is zero, while the shape of the moment–rotation curve is accounted for in an equivalent stiffness of the actuator. As a result,  $k_{tot}$  is estimated from

$$k_{tot} \approx \frac{k_\theta + k_{act}}{N} \quad (6)$$

where  $N$  is the number of links in the joint, and  $k_{act}$  is an equivalent stiffness of a single actuator, taken from a linear fit of the moment–rotation curve shown in Fig. 5 over the range of anticipated link rotation.

The total inertia  $J_{tot}$  is calculated by treating the intermediate links as point masses  $m_L$  with the distance from the center of mass of  $i$ th link to the first flexure being  $L_{L,i}$ , and the total inertia of the final leg structure, incorporating both leg inertia  $J_{leg} = J_N$  and mass  $m_{leg} = m_N$

$$J_{tot} \approx \sum_{i=1}^{N-1} m_L L_{L,i}^2 + J_N + m_N L_N^2. \quad (7)$$

Damping coefficients in micromechanical systems are typically quite difficult to estimate. In the case of the piezoelectric leg joints modeled here, the leg and joint move just a few micrometers above the surface of the surrounding silicon wafer, or substrate, which would typically result in viscous drag being a significant source of damping. In addition, experimental system identification, described in following section, suggested that viscous drag might be a likely source of damping due to the similarity of experimental response to that of a second-order linear system. As a result, a basic estimate of damping coefficient was obtained by integrating the moment due to viscous drag between the underside of the joint and the wafer surface  $M_b$ , and equating it to an effective total damping coefficient  $b_{tot}$ , using the integral

$$M_b = \int_0^{L_{N,out}} \frac{\mu w(r)r}{g} (r\dot{\theta}) dr = b_{tot}\dot{\theta} \quad (8)$$

TABLE II  
VARIABLES FOR LUMPED-PARAMETER MODEL

Parameter	Label	Units	Value
Number of Links	$N$		8
Actuator Stiffness	$k_{act}$	$\mu\text{N/rad/s}$	0.55
Predicted Stiffness	$k_{tot}$	$\mu\text{N/rad/s}$	0.097
Link Mass	$m_{1-7}$	$\mu\text{g}$	1.1
Leg Mass	$m_N$	$\mu\text{g}$	1.7
Leg Inertia	$J_N$	$\mu\text{g}\cdot\text{mm}^2$	15
Link 1 Distance	$L_{L,1}$	$\mu\text{m}$	220
Link 2 Distance	$L_{L,2}$	$\mu\text{m}$	440
$\vdots$	$\vdots$	$\vdots$	$\vdots$
Link 7 Distance	$L_{L,7}$	$\mu\text{m}$	1540
Link 8 (leg) Inner Radius	$L_{N,in}$	$\mu\text{m}$	1760
Link 8 (leg) CoM Distance	$L_N$	$\mu\text{m}$	2700
Link 8 (leg) Outer Radius	$L_{N,out}$	$\mu\text{m}$	4300
Predicted Inertia	$J_{tot}$	$\mu\text{g}\cdot\text{mm}^2$	49
Viscosity	$\mu$	$\text{mN}\cdot\text{s}/\text{m}^2$	0.02
Leg width	$w_{leg}$	$\mu\text{m}$	90
Joint Gap to Substrate	$g_i$	$\mu\text{m}$	2-40
Predicted Damping	$b_{tot}$	$\mu\text{N}\cdot\mu\text{m}/\text{rad/s}$	2-4

where  $r$  is the radius from the base of the joint,  $L_{N,out}$  is the outermost point on the joint and leg structure,  $\mu$  is the dynamic viscosity of air,  $w(r)$  is the width of the joint as a function of radius from the base,  $g$  is the gap between the underside of the leg and the ground, and  $r\dot{\theta}$  is the approximate linear velocity of points along the leg. This type of drag depends heavily on the precise gap between each link in the joint and the substrate, and for a system of smaller links and one long leg link at the end is approximately equal to

$$b_{tot} \approx \sum_{i=1}^{N-1} \frac{\mu A_{L,i} L_{L,i}^2}{g_i} + \int_{L_{N,in}}^{L_{N,out}} \mu \frac{w_{leg} r^3}{3g_N} \quad (9)$$

where  $A_{L,i}$  is the planar area of the  $i$ th link,  $g_i$  is the gap between the  $i$ th link and the ground,  $L_{N,in}$  and  $L_{N,out}$  are the distance from the first flexure to the inner and outer dimensions of the leg (the final,  $N$ th link), and  $w_{leg}$  is the width of the leg. Unfortunately, the gaps  $g_i$  are difficult to predict, being dependent on residual stress in the completed legs, although it can be taken as having an approximately linear increase along the links, from approximately  $0.5 \mu\text{m}$  at the first link to gaps between  $0.5$  and  $40 \mu\text{m}$  at the leg link itself.

Values of the parameters used to predict system dynamics are shown in Table II. The estimated total spring stiffness and moment of inertia correspond to a natural frequency  $\omega_n$  of approximately  $1880 \text{ rad/s}$ , and damping ratio between  $2\%$  and  $20\%$  depending on specific gap widths due to residual stress. These estimates are useful for both refining the design of future leg joints, and anticipating sampling and response time need for driving circuitry and controllers, in this case indicating sampling time for discretization on the order of  $100 \mu\text{s}$  or less, and ideal switching-circuit response time, an order of magnitude or more smaller than that. Note also that sampling rate refers to the rate at which inputs may be changed, not any sensing measurements, as the system is run in open loop under the following control scheme in order to conserve energy. In practice, a  $100 \mu\text{s}$  sampling rate was used for microscale actuator experiments, with the switching circuit described in the following having a response time of less than  $2 \mu\text{s}$ .

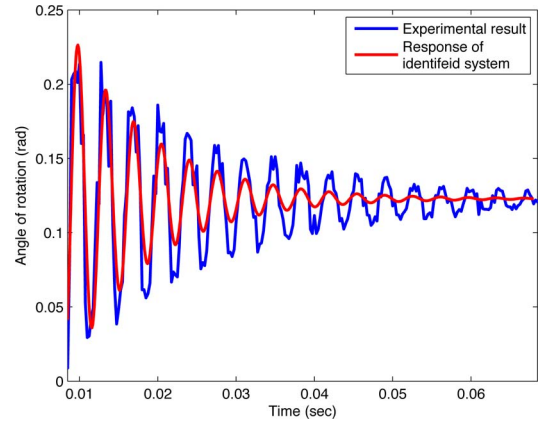


Fig. 7. Step response of the MEMS actuator, which was used for system identification.

### C. Experimental System Identification

Exact system dynamics were measured experimentally using the step response of the completed leg joints. Joint motion was measured by filming the microscale leg joints through a stereoscope using a high-speed camera system. Images were collected at  $4000$  frames per second, and angle measurements in each frame were extracted using the MATLAB Image Processing Toolbox. The measured response and an identified second-order model response are shown in Fig. 7. The identified natural frequency was  $1770 \text{ rad/s}$ , while the identified damping ratio was  $5.7\%$ .

These identified parameters fit in well with the estimated response of the system, given uncertainties in MEMS processing accuracy, and indicate the utility of approximated lump-parameter modeling of the piezoelectric leg joints, although some nonlinearity in the system step response appears to be present, which is likely a result of nonlinear piezoelectric behavior (discussed in the following) and unmodeled damping effects, such as variation in gap between the joint and the substrate as the joint rotates; there is a slight upward deflection of the actuator (approximately  $1-2^\circ$ ) due to residual stress in the thin films on the surface of the actuator. This, and etch holes remaining from the actuator fabrication process mean that the gap between the underside of the actuators and the substrate surface is not entirely constant, as is assumed to estimate the approximate linear damping coefficient. In particular, the gap between joint and substrate is larger at the deflected position, leading to a lower effective damping coefficient near the final position than the initial position during a step displacement.

In addition, changes in system parameters with environmental conditions, and hysteresis of piezoelectric materials can cause the real system to deviate from models used for controller development. For example, the deflection of the piezoelectric actuators is sensitive to temperature, and there is also a modest hysteresis in the piezoelectric actuators, as shown in Fig. 16. We will discuss methods of improving robustness of the actuator response under open loop on-off control when uncertainty is present in controller design. Namely, we treat the stiffness and damping of the system as having approximately  $10\%$  uncertainty

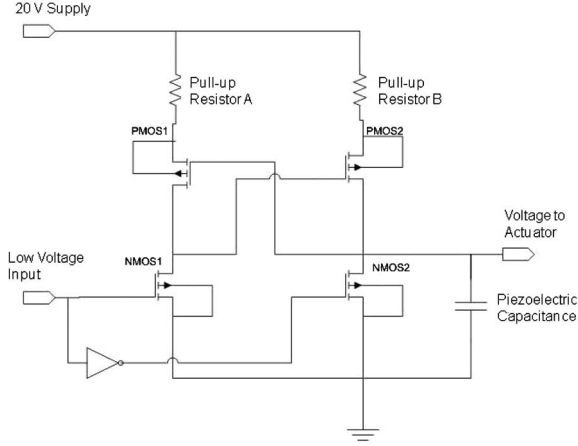


Fig. 8. Switching drive circuit with pull-up resistors to limit leakage current.

due to nonlinearities, hysteresis, or environmental changes and attempt to minimize worst-case error in final position under this uncertainty. These uncertainty bounds may be increased if larger variation is anticipated, but with corresponding reduction in accuracy; systems subject to large parameter variation would require some use of feedback if improved accuracy is required, although this would increase total actuator power consumption.

### III. DRIVE CIRCUIT DESIGN AND TESTING

#### A. Circuit Design

To limit switching losses in the interface between a low-voltage controller and the comparatively high-voltage actuators, a low power on-off switching circuit was designed to interface the two elements. As this interface can cause a significant portion of the switching energy losses for microscale actuators, it is important to be able to predict and measure these losses for incorporation into controller design, as well as to improve performance of the overall system.

The on-off switching circuit designed for the thin-film piezoelectric actuators consists of a CMOS inverter with a level shifter. CMOS inverters are a commonly used switching circuit configuration in the integrated circuit design area for reducing power consumption because in the ideal case, there is no static current and power is consumed only at the “on” or “off” transition time. However, a CMOS inverter alone cannot be used directly for driving piezoelectric actuators. While a piezoelectric actuator should be driven at 20 to 30 V or more, most IC circuits, as are typically used to implement a control law, operate at 5, 3.3 V, or less. Therefore, a level shifter based on the CMOS inverter was designed to interface between a high voltage and a conventional IC process [23]. In order to reduce the power consumption of the circuit, two resistors are added to the basic-level shifter. The conceptual circuit is shown in Fig. 8.

The novel addition of these resistors to the inverter helps to reduce peak leakage current during the switching transitions. While this loss is typically of little consequence when using larger actuators, it can be a substantial portion of energy consumption when working with microscale piezoelectric actua-

tors having comparatively small capacitance. The total energy consumption  $E_{tot}$  due to the circuit alone for a single cycle (charging and discharging of the actuator) can be derived from the energy consumed by transistor capacitance  $E_{C_m}$  and the energy consumed in leakage through the right and left sides of the bridge upon switching  $E_A$  and  $E_B$

$$E_{tot} = E_{C_m} + E_A + E_B \quad (10)$$

with the respective powers being calculated from

$$E_{C_m} = 2C_m U_{low}^2 \quad (11)$$

$$E_A = \frac{(C_L + C_m)(U_{max} - V_{tp} - V_{tp} \log(U_{max}/V_{tp}))}{K_g} U_{max} + \frac{(U_{max} - V_{tp})R_1 C_m V_{tn}}{K R_2 V_{tn}} \quad (12)$$

$$E_B = \frac{C_m (U_{max} - V_{tp} - V_{tp} \log(U_{max}/V_{tp}))}{K_g} U_{max} + \frac{(u_{max} - V_{tp})R_1 C_m V_{tn}}{K R_2 V_{tn}} \quad (13)$$

assuming that the low voltage achieved by the switching circuit is zero, and where  $C_m$  is the capacitance of the MOSFET transistors,  $U_{low}$  is the low-voltage input level of the controller,  $U_{max}$  is the high-voltage “on” voltage to the actuators,  $V_{tp}$  is the threshold voltage of the PMOS transistor in the circuit,  $V_{tn}$  is the threshold voltage of the NMOS transistor in the circuit,  $R_1$  is the pull-up resistor resistance on the low-voltage CMOS inverter,  $R_2$  is the pull-up resistor resistance of the high-voltage CMOS inverter,  $C_L$  is the load capacitance of the piezoelectric actuators, and  $K_g$  is the gain coefficient of the transistors.

The piezoelectric joints have a total capacitance of approximately 1.1 nF, while the transistors utilized had threshold voltages of 1 V, capacitance of 0.23 nF, and gain coefficient of 1.99. Pull-up resistors of 100 and 1000  $\Omega$ , respectively, were used to balance response time of the circuit with low-power consumption, while using readily available surface mount resistors. These parameters correspond to a projected energy consumption of the circuit alone of 1.02  $\mu$ J per charge and discharge cycle, with 0.84  $\mu$ J lost due to leakage current and the remainder due to capacitive loading of the CMOS transistors’ gate capacitance.

### IV. CONTROLLER DESIGN

#### A. System Dynamics and Constraints

As described earlier, the dynamics of the single leg are modeled as a second-order linear system, which can be discretized and represented in state space form as follows:

$$x((k+1)T_s) = A_d x(kT_s) + B_d u_k \quad (14)$$

$$y(kT_s) = C_d x(kT_s) \quad (15)$$

where the states of the system are the angle of rotation ( $\theta_{tot}$ ) and the angular velocity ( $\dot{\theta}_{tot}$ ) of the leg. The discrete time state matrix is  $A_d$ , input matrix is  $B_d$ , and output matrix is  $C_d$ . There are two important constraints on the system when using on-off control. The first is that the inputs  $u_k, k = 1, 2, \dots, n$

can take only two values, namely  $\{0, 1\}$ . Second, the transitions between input values can take place only at the sampling instants, meaning  $u_k$  can change its value only at these times. These constraints limit the reachable subspace of the system in a given time duration.

### B. Problem Statement and Optimization Procedure

The unavailability of feedback and aforementioned input constraints limits the capabilities of this system. So, the limited objective of a controller is to make the leg joint rotate to a desired angle and stay stationary at least instantaneously at the end of a desired time, which will enable the robot to walk in a quasi-static manner.

Mathematically, then, the aim here is to find a sequence of inputs  $u_k, k = 1, 2, \dots, n$ , which, if a solution exists, will move the states of the system from a specified set of initial states to an  $\epsilon$  ball containing a set of desired final states  $x_d$  in a given time  $t_f = nT_s$  (which limits the possible number of transitions between the input states), using minimum energy. The final-state constraints can be written mathematically as  $x_d - \epsilon \leq x(t_f) \leq x_d + \epsilon$ .

Our objective function is then to minimize energy consumption, while satisfying the aforementioned constraints. Energy consumption consists of two parts  $J_C$  and  $J_R$ , corresponding to capacitive and resistive energy losses in the system, respectively. The piezoelectric actuator acts as a capacitor in an electric circuit. Hence, the major part of the energy loss happens when actuators are charged or discharged. This corresponds to a transition of  $u_k$  from 0 to 1 or *vice versa*. This energy loss is termed as capacitive loss or  $J_C$ . In a general on-off control case, the quantity  $CU_{\max}^2/2$  can be replaced by an arbitrary "cost-to-switch"

$$J_C = \sum_{k=1}^n \frac{1}{2} CU_{\max}^2 ((u_k - u_{k-1})^2 + u_0^2) \quad (16)$$

where  $C$  is the capacitance of the piezoelectric actuator and  $U_{\max}$  is the 'on' voltage applied to the actuators.

The second part of the objective function  $J_R$  includes energy lost to resistive dissipation due to leakage current in the on-off drive circuit or through the piezoelectric actuator, and is given by

$$J_R = \sum_{k=0}^n \frac{U_{\max}^2}{R} T_s u_k \quad (17)$$

where  $R$  is the resistance of the system. In other words, this is the energy required for keeping  $u_k$  at 1. Again, here the quantity  $U_{\max}^2/R$  can be generalized to an arbitrary "cost-to-hold."

The optimization problem is to minimize the total energy cost  $J = J_C + J_R$  subjected to state-dynamics constraints ( $n$  constraints), binary constraints, and final-state constraints given earlier. Since the final state is the only point of interest here, the state dynamics can be calculated outside the optimization (18) and can be combined to the final-state constraints

$$x(t_f) = x(nt_s) = \sum_{i=0}^{n-1} A_d^{n-i-1} B_d u_i. \quad (18)$$

TABLE III  
NOMINAL VALUES FOR THE PARAMETERS USED FOR THE DESIGN OF OPTIMAL SEQUENCES FOR THE SYSTEMS

Parameters	Simulation Model	Macro System	MEMS Leg Joint
R ( $\Omega$ )	$3 * 10^9$	$3 * 10^9$	$3 * 10^9$
C (F)	$1 * 10^{-9}$	$1 * 10^{-9}$	$1 * 10^{-9}$
$U_{\max}$ (V)	20	20	20
J (kg.m <sup>2</sup> )	$1.4 * 10^{-12}$	1	$1.4 * 10^{-12}$
b (N.m.s/rad)	$3.4 * 10^{-11}$	14	$2.7 * 10^{-10}$
k (N.m/rad)	$3.2 * 10^{-6}$	40350	$4.4 * 10^{-6}$
G (N.m/V)	$8 * 10^{-8}$	64151	$2.8 * 10^{-8}$
Sampling time ( $T_s$ )(sec)	0.0001	0.001	0.0001

Now, the final-state constraints take the form

$$x_d - \epsilon \leq \sum_{i=0}^{n-1} K_i u_i \leq x_d + \epsilon \quad (19)$$

where

$$K_i = A_d^{n-i-1} B_d.$$

The total energy consumption can be rewritten as follows:

$$\begin{aligned} J &= J_C + J_R \\ &= \sum_{k=1}^n \frac{1}{2} CU_{\max}^2 ((u_k - u_{k-1})^2 + u_0^2) + \sum_{k=0}^n \frac{U_{\max}^2}{R} T_s u_k. \end{aligned} \quad (20)$$

Now, this problem is a binary programming problem with a quadratic objective function (20) and a system of linear constraints (19). Hence, it can be modeled directly in dynamic programming software such as A Mathematical Programming Language (AMPL) and solved using the integer-programming solver CPLEX, which uses the branch and bound technique to integer programming. The parameter values used for optimization are given in Table III.

### C. Modification to Find a Robust Sequence

Uncertainty in the inertia, damping and stiffness estimates (either from analytical or experimental methods) affects the performance of the system, as does variation in actuator behavior due to environmental changes. It is useful to minimize the error for the worst-case system with a bounded uncertainty  $\Delta_{\text{bound}}$ . This is a minimax problem, which can be represented as the following:

$$\min_u \{ \max_{\Delta} \|x_1 - x_{1n}\| \}, \|\Delta\| \leq \Delta_{\text{bound}}. \quad (21)$$

Since the direct solution of this is numerically infeasible, the algorithm given in Fig. 9 and described in the following was developed to find an input sequence that gives a satisfactory performance.

Two optimization techniques are employed here. Continuous nonlinear optimization for determining the worst-case systems ( $\Delta$  values) and binary programming for finding the best robust input sequence. In this particular problem, three parameter uncertainties are considered, namely  $\Delta_m$ ,  $\Delta_b$ , and  $\Delta_k$

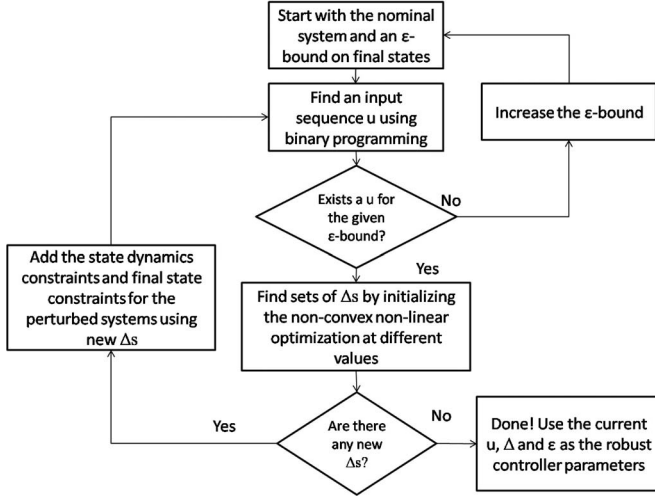


Fig. 9. Robust sequence algorithm.

corresponding to uncertainties in inertia, damping, and stiffness. It is assumed that these uncertainties are bounded on either sides. But, the maximization of error with respect to the  $\Delta$ s is not a convex optimization. Hence, the optimization was initialized at a number of values and the corresponding worst-case system for each was found. For the procedure, let  $(A_1, B_1), (A_2, B_2), \dots, (A_m, B_m)$  be the dynamics of each of the worst-case systems obtained by the maximization. Then, the final-state constraints for all  $m$  systems are added to the binary programming to find the robust  $u$  as follows:

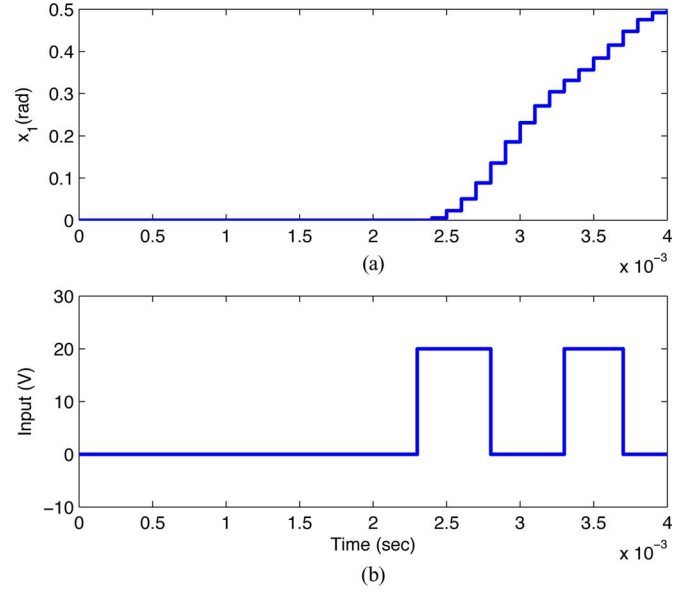
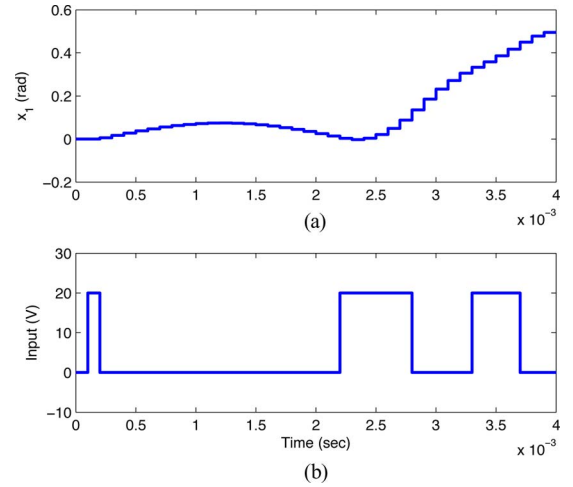
$$\begin{aligned}
 x_d - \epsilon &\leq \sum_{i=0}^{n-1} A_1^{n-i-1} B_1 u_i \leq x_d + \epsilon \\
 x_d - \epsilon &\leq \sum_{i=0}^{n-1} A_2^{n-i-1} B_2 u_i \leq x_d + \epsilon \\
 &\vdots \\
 x_d - \epsilon &\leq \sum_{i=0}^{n-1} A_m^{n-i-1} B_m u_i \leq x_d + \epsilon. \quad (22)
 \end{aligned}$$

These constraint equations help the designer to identify a specific input sequence  $u$  such that if it exists, it will keep the final states of all the aforementioned systems within some  $\epsilon$  neighborhood of the desired final state.

## V. SIMULATION RESULTS

$$J\ddot{\theta} + b\dot{\theta} + k\theta = Gu. \quad (23)$$

The system given in (23) and the corresponding parameters are given in Table III was used for initial simulational study. A couple of sample system responses using the minimal energy open-loop on-off optimal controller is given in Figs. 10 and 11. In these examples, a single leg link is driven to a desired final angle. When only a single leg link is to be controlled, the control

Fig. 10. Sample simulated system output using optimal on-off controller with loose positioning constraint, showing (a) output angle and (b) system input  $u$ .Fig. 11. Sample system output using optimal on-off controller with strict positioning constraint, showing (a) output angle and (b) system input  $u$ .

input can be quite simple, as in the example shown. In Fig. 10, the input switches twice and when the constraints on states are stringent the controller needed three switches, as shown in Fig. 11, which corresponds to a cheaper controller or higher state cost as in linear-quadratic Gaussian (LQG) controller terminology. To explore controller behavior, this on-off controller was compared to the LQG controller for the system, had feedback and analog rather than on-off inputs been available. Two LQG responses corresponding to cheap and expensive controllers are given in Figs. 12 and 13. Both the on/off and LQG controllers produce qualitatively similar trajectories from the initial to the final value. In addition, the capacitive portion of the cost functions from the respective controllers is found to be less for the optimal on-off controller, due to the minimal number of transitions that it dictates. The PZT actuators used in the prototype system have very large resistance, such that over 99% of energy

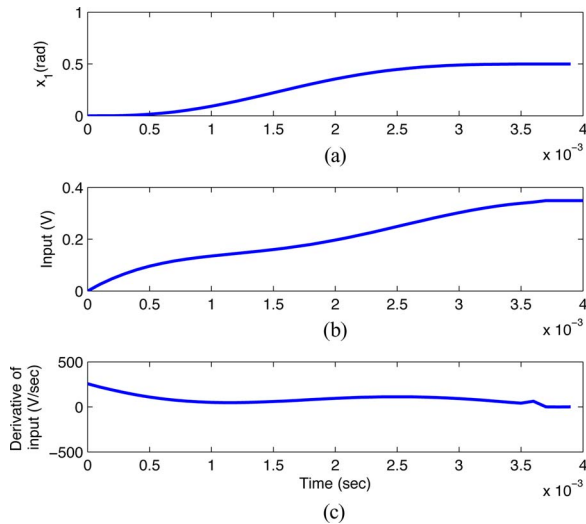


Fig. 12. Simulated LQG response with a cheap controller, analogous to strict positioning constraint, showing (a) output angle, (b) system input  $u$ , and (c) derivative of input.

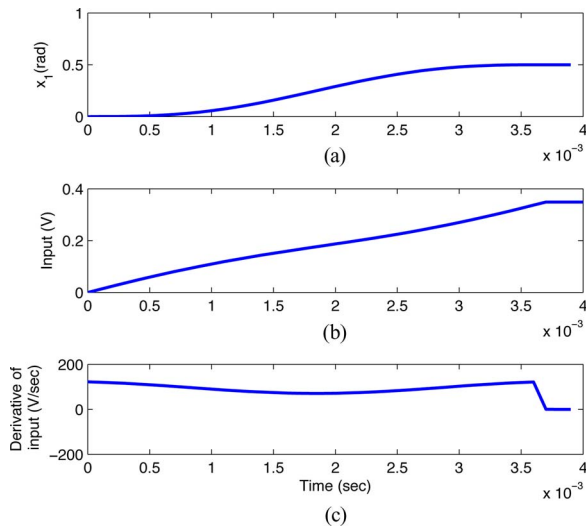


Fig. 13. Simulated LQG response with an expensive controller, analogous to a loose positioning constraint, showing (a) output angle, (b) system input  $u$ , and (c) derivative of input.

use is due to capacitive switching losses, as opposed to resistive holding losses.

The following studies are done to make sure that the optimization is indeed optimal and it can perform effectively in the presence of uncertainty in the system parameters or disturbances.

#### A. Comparison to Brute Force Methods

To ensure that the optimization method is working properly, the result of the efficient optimization method was compared with that of brute force optimization for a shorter time period. In the brute force method, all possible combinations of  $u_i^j$ s were checked for feasibility and that with lowest cost, measured by the on-off cost function, was selected. This approach is, of course, numerically inefficient, as one must check the cost for

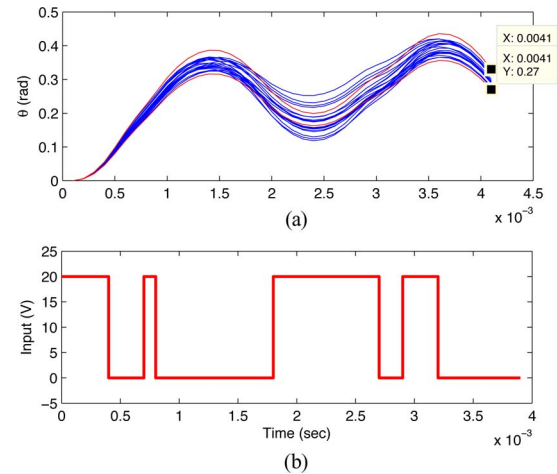


Fig. 14. (a) Response of the perturbed systems when a robust sequence is applied; the red lines show the worst case systems. (b) Corresponding robust on-off sequence.

$2^n$  combinations of input, making it impractical for a larger time period. However, it is possible to verify that for our sample system, the result of the brute force method matches the result obtained by the branch and bound optimization method, which is computationally much more efficient. Over the shorter time period analyzed, the optimal control sequence identified by integer programming exactly matched the best of all possible control sequences tested through the brute force method.

#### B. Robustness Analysis Results

From the simulations, it was found that if the parameter variation (in all parameters) is within 10% of the nominal value for the sample system, then it was possible to find an on-off sequence, which keeps the final state within 10% of the desired final state. This range of parameter uncertainty is sufficient to account for hysteresis in the piezoelectric response, variation in the damping coefficient during leg motion, and potential change in piezoelectric properties over an approximately  $10^\circ\text{C}$  range. Examples of perturbed systems are shown in Fig. 14. When the parameter variations are kept within  $\pm 10\%$  of nominal values, the final states of the randomly perturbed system are within  $\pm 10\%$  of the nominal value,  $0.3 \pm 0.03$ , and this was consistent over the situations we examined.

#### C. Behavior of the System in the Presence of Disturbance

A natural limitation of open-loop control is its inability to reject disturbances. Additional simulation studies were performed to explore the sensitivity of the leg joint under open-loop on-off control to disturbances. While an external force is difficult to apply to the experimental system due to its small size, simulated behavior of the system in the presence of various disturbance, such as due to gravity when the system is tilted, friction forces or electrostatic forces, can be examined. In the sample simulation result shown, ideal dynamic friction between the leg and the ground was considered as a disturbance. A normal force between leg and ground of 5 mN and coefficient of dynamic

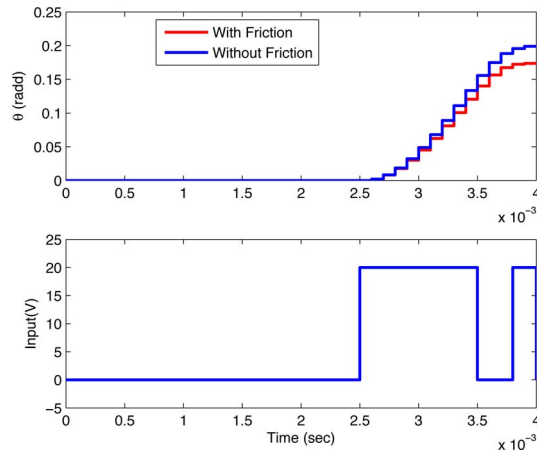


Fig. 15. Comparison between the nominal response and response in the presence of ideal friction.

friction of 0.3 were assumed to be present. The deviation in response from the nominal response of the simulated system is shown in Fig. 15, with an approximately 15% reduction in displacement. As this normal force is much larger than the payload capacity of the leg (5–50 mg, corresponding to approximately 0.5 mN) and much larger than electrostatic forces operating over the displacement range of the leg, there is reason to believe that disturbance forces that would not cause damage to the leg joint result in comparatively small errors. This is primarily a consequence of the large forces for this scale generated by the thin-film piezoelectric actuators. On the other hand, because there is no feedback available, the system has limited capacity to perform a disturbance rejection to reduce this positioning error. When energy constraints are so strict as to preclude sensor use, as may be the case for a microrobot, the additional positioning error must be accepted. However, if occasional sensor measurements can be made, it may be possible to adapt the input on–off sequence over multiple movements, or to switch between optimized on–off sequences if a disturbance is detected, in order to respond to disturbances or environmental changes.

## VI. EXPERIMENTAL RESULTS

### A. Experimental System Description

Experimental testing of the on–off control algorithm was tested on both a macroscale piezoelectric test actuator and the prototype MEMS leg joint. Before conducting the experiments on the MEMS actuator, the control scheme was tested on a macroscale piezoelectric actuator to verify the controller design procedure. The macroscale actuator was a 40-mm-long, 10-mm-wide Ceratec, Inc. bimorph actuator with a strain gauge attached to it for measuring the deflection in terms of the voltage through its sensing circuitry. The on–off switching sequence was loaded into a TMS320F28335 microprocessor, which was interfaced to the bimorph actuator through the fast-switching circuit explained in the previous section. The output voltage was measured using a Tektronix TDS2024B oscilloscope and data was captured using National Instruments Signal Express Tektronix Edition Software. From the step response of the sys-

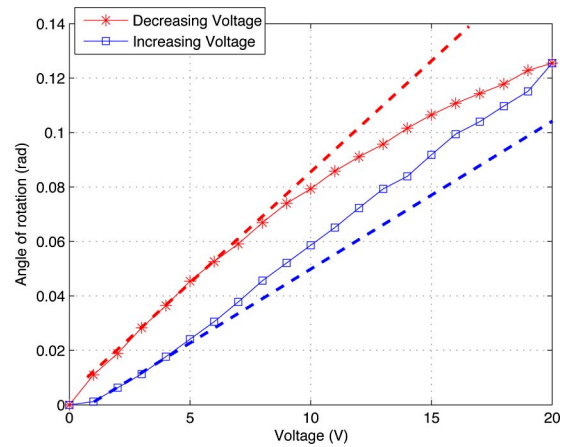


Fig. 16. Hysteresis curve for the MEMS actuator with the dotted lines showing the variation in slope.

tem, the following second-order system given was identified between input voltage and strain gauge voltage:

$$\frac{y(s)}{u(s)} = \frac{64151}{s^2 + 14s + 40350}. \quad (24)$$

The MEMS actuator was also operated using the microprocessor and the switching circuit. Prototype joint arrays were connected to the switching circuit using ultrasonic wire bonding to bond pads at the base of the actuator, on the fixed portion of the substrate. The switching circuit was driven by the microprocessor or a function generator, as appropriate. The motion of the leg was captured using a high-speed camera at 4000 frames per second and the angle of rotation was measured using the MATLAB Image Processing Toolbox. Using the step response given in Fig. 7, a second-order system was identified between the input voltage and the angle of rotation (radians)

$$\frac{y(s)}{u(s)} = \frac{1.9656 \times 10^4}{s^2 + 2 \times 0.0547 \times 1766.4s + 1766.4^2}. \quad (25)$$

To measure hysteresis, a static input voltage was varied from 0 to 20 V and back, giving the hysteresis plot in Fig. 16. This hysteresis effect is included as an uncertainty in stiffness for designing a robust sequence, which is used in the experimental result discussed in the next section.

### B. Comparison of Experimental and Simulation Results

A comparison of the responses from the macro system is shown in Fig. 17. The optimization constraint on final output in this example was to reach  $0.5 \pm 0.1$  V in strain gage output at 20 ms. A binary optimization was done on the identified macro system given in (24) to obtain the input sequence shown in Fig. 17(b) and the constraints are verified using the MATLAB simulation shown. The same input sequence was applied on the macro system and is shown in Fig. 17(a). The experimental response follows very closely with the simulation and reaches 0.58 V at the desired time.

A similar approach with additional robustness constraints to account for hysteresis effects was applied to the MEMS actuator given in (25). In the optimization, the constraints were

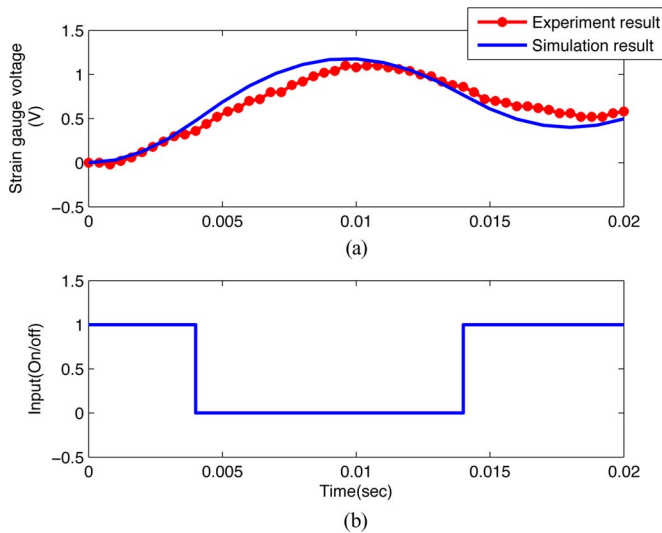


Fig. 17. Comparison of results obtained by experiment and simulation for the macroscale system and the corresponding switching sequence.

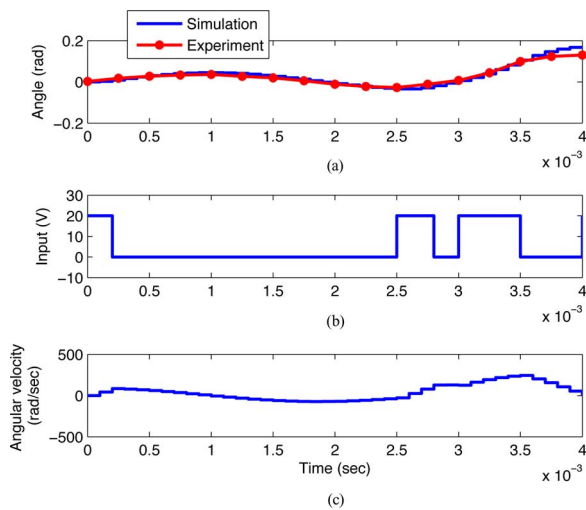


Fig. 18. (a) Comparison of displacement results obtained by experiment and simulation for the MEMS system when under an optimal on-off sequence for 0.15 rad final displacement. (b) On-off voltage input applied. (c) Angular velocity observed in the simulation, showing successful return to 0 rad/s at final time.

applied on both angle of rotation as well as angular velocity at 4 ms for all the perturbed systems with stiffness varying between  $k_{\min} = 127.906$  V/rad to  $k_{\max} = 190.476$  V/rad, which is about  $\pm 20\%$  of the nominal value  $k_{\text{nominal}} = 158.73$  V/rad. The requirement was to make the angle of rotation reach  $0.15 \pm 0.03$  rad and angular velocity reach  $0 \pm 1$  rad/s. From the optimization, it was found out that the minimum possible tolerance on angle is  $\pm 0.03$  rad because of the 20% uncertainty in the stiffness value. The input sequence and simulation responses shown in Fig. 18 were obtained as a result, which satisfies all the constraints in the simulation. When the same sequence was applied on the physical system, the response shown with a red line was obtained. The experimental result follows the simulation result closely and reaches about 0.1115 rad at the stipulated time, which is very close to the expectation from the simula-

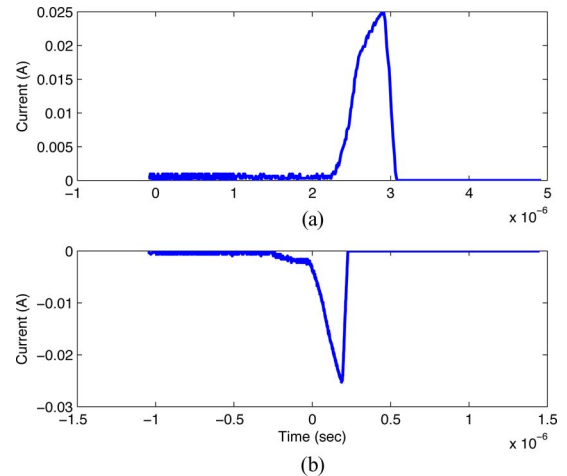


Fig. 19. Current consumption of switching circuitry and the MEMS actuator while the switch is (a) turned on and (b) turned off.

tion (misses the constraint by 0.0085 rad). Also, the direction of rotation reverses in the same video frame, indicating that the angular velocity goes through zero verifying the final-velocity constraint. The discrepancies between the experimental and desired motions are a result of nonlinearity of the actual system, particularly hysteresis in the piezoelectric film. The robust design approach aids in ensuring states are near desired final values even in the presence of model error, but does not ensure any particular accuracy at intermediate times.

During this experiment, the cumulative energy consumption of the microrobotic leg together with the switching circuitry was also measured. The current profiles, while the switch was turned “on” and “off” were measured using a current probe and oscilloscope and are shown in Fig. 19. The power supply was kept constant at 20 V during the entire experiment and each turning “on” cost  $4.6 \times 10^{-7}$  J and each turning “off” consumed  $1.4 \times 10^{-7}$  J. Of this quantity,  $2.2 \times 10^{-7}$  J is attributed to charging at the microactuator, resulting in total energy loss in the circuit alone of just  $3.8 \times 10^{-7}$  J per cycle (the difference between total “on” and “off” energy usage and the energy required to charge the piezoelectric capacitance). This is smaller than the predicted energy usage, which appears to be due to additional resistance within the leg between electrodes for the leg and the piezoelectric actuators; the extra resistance further increases the effect of the pull-up resistors included in the circuit design. Total power consumption of a robot using this controller would depend on step frequency, but for walking gates of 20 Hz or lower, power consumption would be in the tens of microwatts or smaller. This is within the power availability we predict for a microrobot based on piezoelectric actuators, and much smaller than power consumption of an analog controller or PWM controller with much higher switching frequencies.

## VII. DISCUSSION

Although the optimal control method discussed earlier can be extended to include feedback by using a model predictive control approach, the use of open-loop on-off control to

regulate the motion of a piezoelectric actuator is driven entirely by the need to ensure extremely low-power consumption from the entirety of a servo control system. This results in significant tradeoffs in performance for the sake of power reduction. The simple switching interface between controller and actuators, and small number of transitions utilized, allows for control of microactuators that act primarily as a capacitive load with very little energy consumption, less than a microjoule per leg motion. However, such a controller explicitly forgoes the use of feedback to improve response time, robustness, or other closed-loop controller benefits due to power limitations, and the relatively low-switching frequency results in oscillatory output motions with specific desired output states being achieved only at a specific time. In addition, switching controllers may often excite high-frequency dynamics, though this is not a large effect in the experimental test actuators examined here. If present, higher order dynamics may be incorporated into the optimization procedure described here by expanding the system order, but the controller will only act to ensure that these dynamics do not influence behavior at the final time, not to avoid vibration or oscillation at intermediate transitions.

The open-loop, on-off control strategy presented here functions best when the system model is well known, and disturbances or uncertainty in modeling have known and bounded magnitudes. For example, in the MEMS application discussed here, analytical modeling of the piezoelectric rotational joint being controlled is useful in initial actuator design and setting up controller parameters. It may be used to identify necessary sampling periods and on-off drive circuit response times as well as ranges of probable system parameters (such as spring stiffness or damping). However, the accuracy of analytical models is limited by variation in fabrication processes that is difficult to predict before the actuator is completed. For instance, underetching of the silicon layer beneath individual actuators and residual stress in the thin-film piezoelectric and gold layers forming the actuators results in a significant reduction in joint displacement from its ideal performance. In addition, uncertainty in exact etch progress and light upward tilt of the entire joint causes viscous drag on the leg joints to vary over the course of motion, with resulting nonlinear deviations in damping coefficient. Once a leg joint is in use, an experimentally identified model is best used for final controller design. Even so, the on-off controller has no direct ability to adjust to variations in the plant due to environmental changes or external disturbances. It may only be designed, as described in this paper, to minimize error over a range of potential variations and disturbances.

Nonetheless, on-off switching control has a tremendous advantage in terms of power consumption, as switching an on-off signal at select time points requires much less power than analog drive circuitry or high-frequency PWM inputs. Because of its very small energy usage, this controller could provide useful baseline control for autonomous microrobotics. On-off control with a desired final time is especially well suited to quasi-static walking, with multiple legs driven through coordinated motions over a specified time, at which legs in contact with the ground are raised and raised legs lowered for the next step, and absolute precision of an individual leg is not as important as assured forward

progress. In such an application, total inertia of the system would be much larger than that of the leg alone, while damping in the system will depend on the geometry of the body and feet as well as legs. In practice, the environment and loads on the robot may change dramatically, requiring some level of adaptation or feedback. A variety of optimized on-off sequences under different load conditions may be stored for use, or the optimal on-off sequence may serve to initiate adaptive control using only occasional or very low frequency sensor feedback to make modest adjustments to the input sequence, while keeping power consumption low.

## VIII. CONCLUSION

The chief conclusions of this paper, then, are based on the idea that while thin-film piezoelectric actuation may one day enable unique mobility capabilities from microscale autonomous robots, achieving directed appendage movements will require aggressive reduction in power consumption throughout the servo control system. In this paper, we focus on modeling leg dynamics and reducing power consumption by the actuators and in the drive circuit interfacing low-voltage control electronics with a high-voltage actuator supply. In particular, we introduce a simple optimization method for achieving minimum energy on-off control when switching costs are substantial. We have applied the control algorithm to both a macroscale piezoelectric test bed and to prototype microrobotic leg joints, successfully directing the states of the systems to desired target values. In addition, with use of an inverter circuit specifically designed for low-power operation, we can limit leakage current while driving the actuators and obtain our desired motions with just a few microjoules per leg step, within the predicted energy and power limitations of future microrobotic platforms, and well below more conventional control implementations. Controlled motions are completed successfully with better than 10% positioning accuracy given a linear model, and better than 15% in simulation against a disturbance forces greater than 1 mN, and thus, larger than we would expect the actuator to face. However, further improvements in accuracy are difficult given the ultralow power open-loop strategy, such that further robustness to parameter variation or disturbances would require a true feedback implementation, and thus, increased servo system power.

## ACKNOWLEDGMENT

The authors would like to thank R. Piekarz, J. Martin, B. Power, and R. Rudy at the U.S. Army Research Laboratory for their expertise in fabrication of the MEMS actuators.

## REFERENCES

- [1] T. M. Ebefors, U. Johan, E. Kälvesten, and G. Stemme, "A walking silicon micro-robot," in *Proc. 10th Int. Conf. Solid-State Sens. Actuators*, Sendai, Japan, 1999, pp. 1202–1205.
- [2] A. Bonvilain and N. Chaillet, "Microfabricated thermally actuated micro-robots," in *Proc. IEEE Int. Conf. Robot. Autom.*, Taipei, Taiwan, 2003, pp. 2960–2965.
- [3] M. H. Mohhebi, M. L. Terry, K. F. Böhringer, G. T. A. Kovacs, and J. W. Suh, "Omnidirectional walking microrobot realized by thermal microactuator arrays," in *Proc. ASME Int. Mech. Eng. Congr.*, New York, NY, 2001, pp. 1–7.

- [4] S. Hollar, A. Flynn, C. Bellow, and K. S. J. Pister, "Solar powered 10 mg silicon robot," in *Proc. MEMS 2003*, Kyoto, Japan, pp. 706–711.
- [5] B. R. Donald, G. G. Levy, C. D. McGray, I. Papatry, and D. Rus, "An untethered electrostatic, globally controllable MEMS micro-robot," *J. Microelectromech. Syst.*, vol. 15, no. 1, pp. 1–15, Feb. 2006.
- [6] R. J. Linderman and V. M. Bright, "Nanometer precision positioning robots utilizing optimized scratch drive actuators," *Sens. Actuators A, Phys.*, vol. A91, no. 3, pp. 292–300, Jul. 2001.
- [7] K. Oldham, J. Pulskamp, R. Polcawich, and M. Dubey, "Thin-film PZT actuators with extended stroke," *J. Microelectromech. Syst.*, vol. 17, no. 4, pp. 890–899, Aug. 2008.
- [8] K. Oldham, J. Pulskamp, R. Polcawich, P. Ranade, and M. Dubey, "Thin-film piezoelectric actuators for bio-inspired micro-robotic applications," *Integr. Ferroelectr.*, vol. 95, no. 1, pp. 54–65, 2007.
- [9] J. S. Pulskamp, R. G. Polcawich, and K. Oldham, "Millimeter-scale robotics research at the Army Research Laboratory," presented at the ASME Int. Des. Eng. Tech. Conf. Micro- Nano-Syst., San Diego, CA, Sep. 2009.
- [10] W. C. West, J. F. Whitacre, E. J. Brandon, and B. V. Ratnakuma, "Lithium micro-battery development at the Jet Propulsion Laboratory," *IEEE Aerosp. Electron. Syst. Mag.*, vol. 16, no. 8, pp. 31–33, Aug. 2001.
- [11] J. B. Lee, Z. Chen, M. G. Allen, A. Rohatci, and R. Arya, "A miniaturized high-voltage solar cell array as an electrostatic MEMS power supply," *J. Microelectromech. Syst.*, vol. 4, no. 3, pp. 102–108, Sep. 1995.
- [12] M. Sitti, "Piezoelectrically actuated four-bar mechanism with two flexible links for micromechanical insect thorax," *IEEE/ASME Trans. Mechatronics*, vol. 8, no. 1, pp. 26–36, Mar. 2003.
- [13] E. Steltz and R. S. Fearing, "Dynamometer power output measurements of miniature piezoelectric actuators," *IEEE/ASME Trans. Mechatronics*, vol. 14, no. 1, pp. 21–31, Feb. 2009.
- [14] J. A. Main, D. V. Newton, L. Massengill, and E. Garcia, "Efficient power amplifiers for piezoelectric applications," *Smart Mater. Struct.*, vol. 5, no. 3, pp. 766–775, 1996.
- [15] D. Campolo, M. Sitti, and R. S. Fearing, "Efficient charge recovery method for driving piezoelectric actuators with quasi-square waves," *IEEE Trans. Ultrason., Ferroelectr., Frequency Control*, vol. 50, no. 3, pp. 237–244, Mar. 2003.
- [16] P. Galambos, D. Czapski, R. Givler, K. Pohl, D. L. Luck, G. Benavides, and B. Jokiel, "Drop ejection utilizing sideways actuation of a mems piston," *Sens. Actuators A*, vol. 141, pp. 182–191, 2008.
- [17] D. A. Horsley, W. O. Davis, K. J. Hogan, M. R. Hart, E. C. Ying, M. Chaparala, B. Behin, M. J. Daneman, and M. H. Kiang, "Optical and mechanical performance of a novel magnetically actuated MEMS-based optical switch," *J. Microelectromech. Syst.*, vol. 14, no. 2, pp. 274–284, Apr. 2005.
- [18] C. Y. Kaya and J. L. Noakes, "Computational method for time-optimal switching control," *J. Optim. Theory Appl.*, vol. 117, no. 1, pp. 69–92, Apr. 2003.
- [19] W. Singhose, T. Singh, and T. W. Seering, "On-Off control of flexible spacecraft with specified fuel usage," in *Proc. Amer. Control Conf.*, 1997, pp. 2308–2312.
- [20] B. J. Driessen, "On-off minimum-time control with limited fuel usage: Near global optima via linear programming," in *Proc. Amer. Control Conf.*, 2000, pp. 3875–3877.
- [21] A. Bemporad and N. Girogetti, "A SAT-based hybrid solver for optimal control of hybrid systems," *Lect. Notes Comput. Sci.*, vol. 2993, pp. 126–141, 2004.
- [22] M. S. Branicky, V. S. Borkar, and S. K. Mitter, "A unified framework for hybrid control: Model and optimal control theory," *IEEE Trans. Autom. Control*, vol. 43, no. 1, pp. 31–45, Jan. 1998.
- [23] P. H. Saul, K. M. Brunson, and R. J. T. Brunyan, "Versatile high voltage level shift and driver for MEMS applications," *Electron. Lett.*, vol. 39, no. 2, pp. 185–186, 2003.



**Biju Edamana** received the B.Tech. degree in mechanical engineering from the National Institute of Technology, Calicut, India, in 2004, and the M.S. degree in mechanical engineering from the University of Michigan, Ann Arbor, MI, in 2008, where he is currently working toward the Ph.D. degree.

His current research interests include developing low-energy control strategies for microrobotics, under development in the Vibrations and Acoustics Laboratory, University of Michigan.



**Bongsu Hahn** received the B.S. degree in mechanical engineering from Yeungnam University, Gyeongsan, Korea, in 1999, and the M.S. degree in mechatronics engineering from Gwangju Institute of Science and Technology, Gwangju, Korea, in 2002.

From 2002 to 2007, he was a Researcher with the Actuation and Control Team for Missile Guidance, Agency for Defense Development, Korea. Since 2007, he has been with the Vibration and Acoustic Laboratory: Microsystems, University of Michigan, Ann Arbor. His current research interests include low-power switching control for microdevices, coordinating highly efficient voltage conversion, and adaptive control.



**Jeffrey S. Pulskamp** received the B.S. degree in mechanical engineering from the University of Maryland, College Park, in 2000.

He is currently MEMS Design and Mechanical Engineer with the Micro and Nanomaterials and Devices Branch, U.S. Army Research Laboratory, Adelphi, MD. He holds six patents related to piezoelectric MEMS devices. His current research interests include tunable MEMS resonators/filters for secure communication, switches and phase shifters for phased-array antennas, millimeter-scale robotics, device design and modeling of piezoelectric MEMS, RF devices, and MEMS actuators.

device design and modeling of piezoelectric MEMS, RF devices, and MEMS actuators.



**Ronald G. Polcawich** received the B.S. degree in materials science and engineering from Carnegie Mellon University, Pittsburgh, PA, in 1997, and the M.S. degree in materials and the Ph.D. degree in materials science and engineering from the Pennsylvania State University, University Park, in 1999 and 2007, respectively.

He is a Staff Researcher with the Micro and Nanomaterials and Devices Branch, U.S. Army Research Laboratory, Adelphi, MD, where he is currently the Team Leader for the RF MEMS and mm-scale robotics programs. He holds three patents, two of which are related to piezoelectric switches using PZT thin films. He has authored or coauthored more than 30 journal articles and one book chapter on fabrication and design of piezoelectric MEMS devices. His current research interests include switches and phase shifters for phased-array antennas, tunable MEMS resonators/filters for secure communication, mobile unattended sensor platforms, materials processing of PZT thin films, MEMS fabrication, piezoelectric MEMS, RF components, MEMS actuators, and mm-scale robotics.



**Kenn R. Oldham** (M'09) received the B.S. degree in mechanical engineering from Carnegie Mellon University, Pittsburgh, PA, in 2000, and the Ph.D. degree in mechanical engineering from the University of California, Berkeley, in 2006.

He is currently an Assistant Professor in the Department of Mechanical Engineering, University of Michigan, Ann Arbor, MI. His research interests include microactuator design and applications, optimal design and control, design for controllability, and efficient sensing and power strategies for microelectromechanical system devices.

Prof. Oldham is a member of the American Society of Mechanical Engineers.